On the relationship between mechanical energy rate and heat dissipated rate during fatigue for a C45 steel depending on stress ratio

Rosa De Finis*, Davide Palumbo*, Umberto Galietti*

*Politecnico di Bari, Dipartimento di Meccanica, Matematica e Management, Via Orabona, 5-70125 Bari, Italy

Corresponding author: rosa.definis@poliba.it

Abstract

This work deals with the analysis in the frequency domain of the temperature signal and mechanical energy rate of C45 steel under two different fatigue stepwise loading series at stress ratios of 0.1 and -1.

It was first investigated the energy distribution among the harmonic components of the signals to understand possible variations caused by a different stress ratio.

In addition, the second amplitude harmonic (SAH) of heat dissipated and mechanical energy rates have been considered in the analysis and their relationship was investigated. It has been shown as it depends only on the material, hence it is valid whatever the kind of the test is without any assumption on the energy supplied to the material or material hysteresis loop stabilisation.

The adopted approach allows the analysis of intrinsic dissipations by means of rapid, full-field and contactless techniques without any specific requirement on loading condition or temperature signal stabilisation.

Keywords: Fatigue strength, second amplitude harmonic of heat dissipated energy rate, cyclic stress/strain curve, strain energy density

Nomenclature

ρ material density [Kg/m^3]

c_p Specific heat at constant pressure [J/kg K]

σ_a stress semi-amplitude [MPa]

$\Delta T_{2\omega}$ SAH (second amplitude harmonics) of temperature signal [K]

R stress ratio

f mechanical frequency [Hz]

$\dot{E}_d$ heat energy rate dissipated by a unit volume of material [W/m^3]

$\Delta \dot{E}_d$ peak to peak amplitude of the heat energy rate dissipated by a unit volume of material [W/ m^3]

$\Delta \dot{E}_{d1\omega}$ FAH (first amplitude harmonics) of heat energy rate dissipated by a unit volume of material estimated by using the $\Delta T_{2\omega}$ [W/m^3]

$\Delta \dot{E}_{d2\omega}$ SAH (second amplitude harmonics) of heat energy rate dissipated by a unit volume of material estimated by using $\Delta T_{2\omega}$ [W/m^3]

$\dot{W}$ strain energy density rate or mechanical energy rate [W/ m^3]

$\Delta \dot{W}$ peak to peak amplitude of the strain energy density rate [W/ m^3]

$\Delta \dot{W}_{1\omega}$ FAH (first amplitude harmonics) of strain energy density rate [W/ m^3]

$\Delta \dot{W}_{2\omega}$ SAH (second amplitude harmonics) of strain energy density rate [W/ m^3]

W_p strain energy density per cycle or area under hysteresis loop [J/m^{3}cycle]

$\dot{E}_s$ stored energy rate [W/ m^3]

$\dot{Q}$ heat energy rate exchanged by a unit volume of material [W/ m^3]

$\dot{U}$ rate of variation of internal energy per unit volume of material [W/ m^3]

f_c sampling frequency of mechanical data [frame/s]

φ phase shift between stress and strain [rad]

1.Introduction

It is well-established that during cyclic loading, the energy is dissipated because of plastic deformations and a portion of this energy is converted into heat while another portion is irrecoverable at every cycle due to the plastic strain energy absorption [1-10].

The energy dissipated in the material (cyclic plastic energy) because of mechanical loading, is related to the number of cycles for failure and can be used as a damage parameter for the material fatigue life estimation [4-6]. Such an energy dissipation is of critical importance for setting up energy-based fatigue life prediction approaches [10-14] based on the assessment of mechanical energy input [10-19] or heat converted energy by measuring the material surface temperature [20-30].

Even if many efforts have been made to better understand the relationships between surface thermal measurements and heat converted energy, and between heat converted energy and intrinsic dissipations, is still unclear how such relationships vary from a loading condition or regime to another [30-42].

Referring to the assessment of mechanical energy input, the aim is to assess the area under the hysteresis loop that represents the energy dissipated, by investigating the constitutive stress-strain law [9,10] or by modelling the strain hardening behaviour [7,11]. Both the approaches require the definition of a model and the experimental assessment of coefficients (i.e. hardening exponent, coefficient, etc.) that depend on imposed loading, fatigue regime, material. In addition, to

implement these models some assumptions need to be made: the identical tensile/compressive stress-strain behaviour, material cyclic stabilisation (shape and hardening do not change) and absence of ratcheting.

Under an experimental point of view, the energy dissipated can be obtained by strain measurements carried out by means of ad-hoc tests assisted by an extensometer [15-17] or full-field techniques such as the Digital Imaging Correlation (DIC) [18-20]. The first cannot be applied for the real component under operating conditions while the second can be not accurate for a higher loading frequency and low strain values [18-20] and could be not feasible for in-situ applications on components.

The assessment of cyclic plastic energy [3,7] by evaluating heat converted energy via rapid tests and an ease experimental setup [21,31-34] is a valid tool to overcome, as an example, the issues related to the applicability of measurement sensors to the components. La Rosa [19], recently found qualitatively a link between thermal increments and the cyclic plastic energy for AISI 304 steel under stepwise loading at $R=-1$ while Nourian-Avval [23] adopted an approach based on entropy estimations and found that the dissipating energy is directly proportional to the steady-state temperature during a stepwise test for DP steel and 1045 steel (data assessed by literature). However, the steady-state temperature is affected by several 'disturbing heat sources' not strictly related to the fatigue damage, so that suitable processing is required to analyse the data, as explained by [31]. Another interesting point is represented by the ratio between heat converted energy and cyclic plastic energy [26,35-37] that can be supposed unitary only in fully reversed loading conditions while the validity of this assumption in presence of the mean stress in the load has not been yet widely investigated by using thermal methods.

In the last years, several works [25-37] focused their attention on the second amplitude harmonic of the temperature (SAH) as a parameter for estimating the heat dissipated during fatigue [29-32]. De Finis et al. [32-33] by following Enke [27], showed as the decomposition of the temperature signal by using a suitable temperature model allows a multi-analysis of the thermal behaviour by different perspectives. Krapez [30] used the SAH for qualitatively estimating the fatigue limit of metals while Sakagami [29] linked the SAH with fatigue damage in terms of persistent slip bands that lead to crack initiation in AISI 316 steel under a fully reversed load application. De Finis [30] also used SAH during constant amplitude tests of CFRP composites to demonstrate the capability of the parameter for the damage monitoring.

The major part of these works [19,22-23], however, is carried out at a stress ratio of -1, where the SAH is the fundamental dissipative temperature component [25]. To date, no considerations on the ratio between heat converted energy provided by SAH and cyclic plastic energy were made for $R\neq-1$ conditions.

In general, the stress ratio R not only can determine a different thermal-to-mechanical energies ratio [36] but also can influence the way the energy content (mechanical and thermal) distributes among the components of the frequency spectrum. Such an harmonic energy distribution represents important information for understanding the link between thermal and mechanical data and in spite of many valuable works reported in the literature [25-37], more research is still needed to establish the connection between the thermography approach and traditional energy-based approaches.

In the present work, the frequency spectra of mechanical energy rate and heat dissipated energy rate are investigated with the aim of:

- studying the harmonic energy distribution depending on stress ratios,
- investigating the relationship between SAH dependence on stress ratio and loading conditions,
- investigating the capability of SAH of temperature signal as a useful parameter to estimate the heat dissipated energy in different loading conditions.

Two experimental campaigns were set-up: one at $R=-1$ and the other at $R=0.1$, both involving the application to six samples of a stepwise loading sequence up to material failure.

Mechanical data in terms of stress and strain allowed the evaluation of mechanical energy rate and area under hysteresis loop, while temperature data allowed the assessment of the heat dissipated energy rate.

The main novelty of the work refers to the investigation of both the mechanical and the thermal energy rates in the frequency domain and the assessment of a relationship between SAHs. In addition, some considerations between SAH of mechanical energy rate and area under the hysteresis loop were drawn.

The adopted technique is full-field and contactless, involves ease material preparation and a rapid fatigue characterisation.

2. Theory

During fatigue processes a portion of energy supplied to the material converts in heating according to the following energy balance (first Law of Thermodynamic) [24-28,32] in terms of rate of energies [9]:

$$\dot{W}+\dot{Q}=\dot{U}=\dot{E}_s+\dot{E}_d \quad (1)$$

Eq. (8) shows that the sum of mechanical energy rate $\dot{W}$ and the heat energy rate exchanged with environment $\dot{Q}$ is balanced by the rate of variation of internal energy $\dot{U}$ where $\dot{E}_s$is the fraction of energy that does not converts in heating and is related to the accumulation of plastic deformation while $\dot{E}_d$ is heat dissipated energy rate which surface temperature T is a sentinel [32], Fig. 1(a).

The energy during a cyclic process, $\dot{W}$, can be defined by defining stress and strain over time [10]:

$$\sigma(t)=\sigma_m+\sigma_a \sin(2\pi f t) \quad (2)$$

$$\varepsilon(t)=\varepsilon_m(R,\sigma_m)+\varepsilon_a(R,\sigma_a)\sin(2\pi f t-\varphi) \quad (3)$$

where, σ_m, σ_a, ε_m and ε_a are mean and amplitude of the stress, mean and amplitude of the strain, φ the phase shift between stress and strain, f the loading frequency. As it is possible to observe ε_m and ε_a values are clearly dependent on stress ratio (R) and stress amplitude.

A simple viscoelastic model that defines the constitutive stress-strain law [10,11] can be used to draw some considerations on the energy involved in fatigue damage during a stepwise uniaxial loading sequence imposed to samples at two stress ratios. The model provides synthetic data that represent just a reference for comparing experimental results.

By differentiating the strain:

$$\dot{\varepsilon}(t)=2\pi f \varepsilon_a[\cos(2\pi f t)\cos\varphi+\sin(2\pi f t)\sin\varphi] \quad (4)$$

Considering the product between Eq. (2) and Eq. (3), it is possible to assess the mechanical energy rate $\dot{W}$ that is the derivative along the time of work increment of the external forces treated as a scalar product of the instantaneous values of stress and strain [11], also called instantaneous power density [10]:

$$\dot{W}(t)=\sigma(t)\dot{\varepsilon}(t)=\sigma_m 2\pi f \varepsilon_a[\cos(2\pi f t)\cos\varphi+\sin(2\pi f t)\sin\varphi]+\sigma_a\ 2\pi f \varepsilon_a[\sin(2\pi f t)\cos(2\pi f t)\cos\varphi+\sin(2\pi f t)^2\sin\varphi] \quad (5)$$

By considering that the system pulsation is $\omega=2\pi f$, and the relation between σ_{max}, σ_m, σ_a, and R, and by considering that $\varepsilon_a=\sigma_a/E$ [15], it is possible to write:

$$\dot{W}(t)=\omega\ \frac{1-R^2}{4E}\sigma_{max}{}^2[\cos(\omega t)\cos\varphi+\sin(\omega t)\sin\varphi]+\omega\ \frac{(1-R)^2}{4E}\sigma_{max}{}^2[\sin(\omega t)\cos(\omega t)\cos\varphi+\sin(\omega t)^2\sin\varphi]=\ \omega\ \frac{1-}{4}$$

(6)

Eq.(6) shows the mechanical energy rate dependence to stress ratio, stresses, loading frequency and phase shift between stress and strain.

By considering trigonometric addition formulas, Eq. (6) becomes more compact:

$$\dot{W}(t)=\Delta\dot{W}_{1\omega}[\cos(\omega t-\varphi)]+\Delta\dot{W}_{2\omega}[[\sin(2\omega t-\varphi)]+K] \quad (7)$$

where

$$\Delta\dot{W}_{1\omega}=\omega\frac{1-R^2}{4E}\sigma_{max}{}^2 \quad (8)$$

$$\Delta\dot{W}_{2\omega}=\omega\frac{(1-R)^2}{8E}\sigma_{max}{}^2 \quad (9)$$

$$K=\frac{1}{2}\sin(\varphi) \quad (10)$$

From Eq.(7) it is possible to highlight that $\dot{W}$ is a function described by *1ω* and *2ω* components whose amplitudes are respectively $\Delta\dot{W}_{1\omega}$ and $\Delta\dot{W}_{2\omega}$ and an offset represented by *K*. Fig. 1(b), represents graphically the function $\dot{W}(t)$, $\Delta\dot{W}$ that is the peak to peak variation of $\dot{W}$, and the spectral components $\Delta\dot{W}_{1\omega}$ and $\Delta\dot{W}_{2\omega}$ for a specific stress value of the test.

When *R*=-1, the change of $\dot{W}$ during one cycle of stress and strain makes two cycles, and there is a turn of energy input to the system by the work of the external forces [10,25-27]. In effect, the first term of Eq. (5) is null and the only non-zero component is the one running at *2ω*. If *R≥0*, in presence of mean stress, the $\dot{W}$ function shows additional components running at a frequency different from the fundamental one (*2ω*), so that, the energy component related to intrinsic dissipation is also the one running at *1ω*. The presence of just two harmonic components is due to the adopted simplified viscoelastic model. By considering another model, the strain/stress law clearly varies, and other high-other harmonics can be present.

$\dot{W}$ function must be integrated over a period (*T=1/f*) in order to obtain the area under hysteresis loop:

$$W_p = \int_0^T \dot{W}(t)\,dt \tag{11}$$

The W_p value depends on stress ratio, Fig. 1(b), and can be obtained by estimating the heat converted energy (E_d) that in turns can be assessed by analysing the surface temperature of the sample [33,19].

In a previous research, Jordan [26] found a direct relation between the mechanical energy variation (W_p) and heat converted energy during fatigue, while Enke [25] proposed a model to represent the temperature changes where the SAH of thermal signal was the fundamental in presence of damage under a fully reversed loading where the energy is supposed to convert totally in heating.

More investigations are required to understand if the SAH of the temperature signal can be also useful for the estimation of the heat dissipated when the loading condition involves a non-zero mean stress.

In present work, the attention is focused on the study of the SAH of $\dot{E}_d$ and $\dot{W}$ for two stress ratio conditions to understand their relationship by supposing that stored energy rate $\dot{E}_s$ is negligible.

In the same way as $\dot{W}$, the heat dissipated energy rate, $\dot{E}_d$, is a periodic function that can be considered as the superposition of different sinusoidal signals of suitable amplitude and frequency, phase shifted each other:

$$\dot{E}_d(t) = \Delta\dot{E}_{d0} + \sum_{n=1}^{\infty} \Delta\dot{E}_{dn\omega}\sin(n\omega t + \varphi_n) = \Delta\dot{E}_{d0} + \Delta\dot{E}_{d1\omega}\sin(1\,\omega t + \varphi_1) + \Delta\dot{E}_{d2\omega}\sin(2\,\omega t + \varphi_2) + \ldots \tag{12}$$

where $\Delta \dot{E}_{d1\omega}$ represents the amplitude of the first harmonics of heat dissipated rate (FAH) and $\Delta \dot{E}_{d2\omega}$ represents the SAH one while $\Delta \dot{E}_{dn\omega}$ the -nth one and $\Delta \dot{E}_{d0}$ is the mean value. The function has been truncated at the second term for simplicity.

To understand the derivation of such an energy rate, the following considerations on temperature signal are necessary.

In Fig. 1(b)**,** a sketch of the temperature variations during fatigue test at a stress above the fatigue limit or more in general above the elastic limit [39], is reported. In real conditions, the temperature of the steady state is achieved during a balance between the energy supplied and heat exchanges [40,22-23].

Considering a steady state condition, whatever the stress ratio is, the temperature signal spectrum can be represented by a number of harmonic components, for sake of simplicity in Fig. 1(b) are represented just three: the one running at the pulsation 1ω ($\Delta T_{1\omega}$), the SAH component ($\Delta T_{2\omega}$) and the one at 3ω ($\Delta T_{3\omega}$).

Under a fully reversed load, as demonstrated by Enke [25] the fundamental dissipative component is $\Delta T_{2\omega}$ while in presence of the mean stress in the loading, the dissipative components are distributed over other harmonics, i.e. on $\Delta T_{1\omega}, \Delta T_{3\omega}$. In this case, $\Delta T_{1\omega}$ will represent not only the well-known temperature variations related to the thermoelastic effect [32,38] but also the temperature variations related to irreversible processes. In case one would consider also the $\Delta T_{1\omega}$ as damage parameter, it is required to filter out thermoelastic contribution to the temperature.

In present study, we focused the attention on the 2ω temperature variations as a component related to the damage [31-34] useful for estimating the energy dissipated, this allows to investigate the relationship between $\Delta \dot{E}_{d2\omega}$ and $\Delta \dot{W}_{2\omega}$.

The $\Delta \dot{E}_{d2\omega}$ term can be obtained by directly assessing the $\Delta T_{2\omega}$ [32] component of temperature signal, according to the following equation:

$$\Delta \dot{E}_{d2\omega} = f \Delta E_{d2\omega} = f \rho c_p \Delta T_{2\omega} \qquad (13)$$

where $\Delta E_{d2\omega}$ is SAH of the heat energy dissipated by a unit volume of material obtained according to the procedure presented in [31-34], and f is the mechanical frequency. In Eq.(13), ρ is the density and c_p is the specific heat at constant pressure. It is important to underline that $\Delta E_{d2\omega}$represents just an estimation of the total dissipated energy due to the fatigue damage, then it is an index of how much energy is dissipated as heat, that clearly depends on stress ratio.

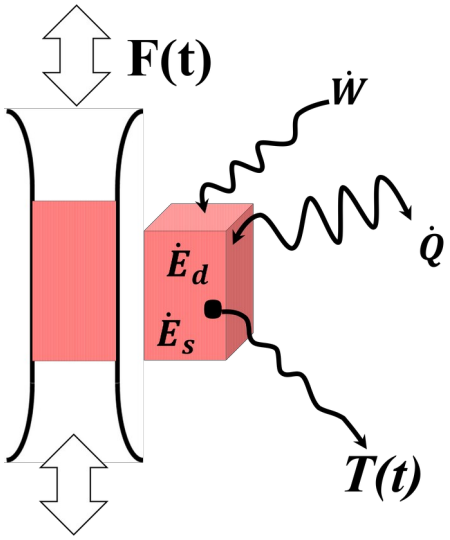

(a)

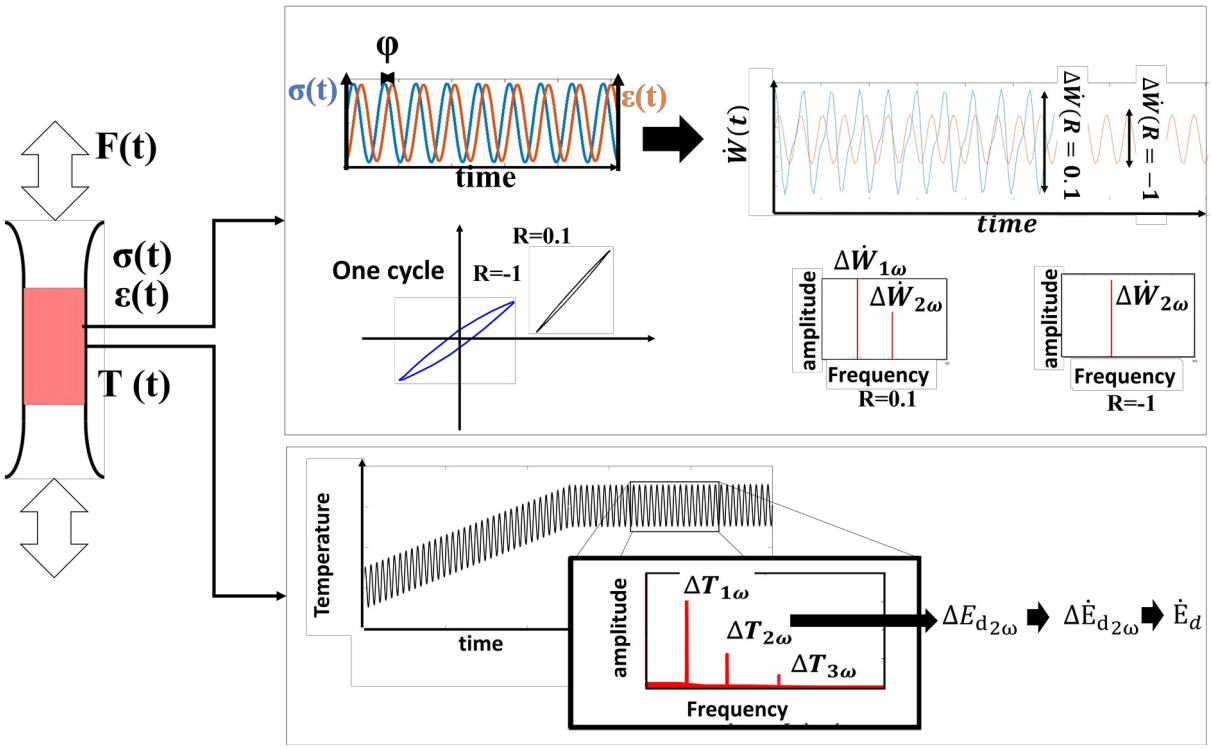

Figure 1. (a) Energies involved during a fatigue process Eq. (1), and surface temperature, (b) sketch of mechanical energy rate and its frequency spectrum and temperature behaviour for stress level above the fatigue limit (σ_{end}) and frequency spectrum

2. Experimental Campaign

2.1. Experimental Tests

The tested material is the EN/DIN C45 steel that presents a good compromise between strength and toughness. It is used in many mechanical applications: shafts, cranks, key cards, hinges, rods, gears.

Thermophysical properties assumed are: $\rho = 7800\, Kg/m^3$, $c_p = 486\, \frac{J}{Kg\, K}$.

The carried out tests are:

- tensile tests (five samples tested), in order to obtain the static characterisation of the C45,
- fatigue tests by using a stepwise loading procedure at *R=0.1* (three samples being tested) and at *R=-1* (three samples being tested). The samples are hereinafter referred to as S_1, S_2, S_3.

Samples geometry and dimensions were according the Standard [41], Fig. 2(a).

The samples for fatigue tests have been preliminarily polished by using acetone while surface asperities and irregularities were removed by using a mechanical air die grinder. Moreover, a matt black coating was applied on the surface to increase the surface emissivity and then improve the acquired thermal signal.

Tensile and fatigue tests were performed with the MTS model 370 servo-hydraulic loading frame (100 kN of capacity) and during the tests the samples were equipped with a clip-on extensometer (gage length 25 mm). Mechanical data from extensometer were acquired by elaborating unit of the loading machine at frequency of 204 Hz.

Tensile tests were performed under displacement control with a rate of 2 mm/min. Estimated Young's modulus, Yield strength and Ultimate Tensile Strength (*UTS*) were respectively 205 MPa (sd.10 MPa), 450 MPa (sd. 25 MPa) and 760 MPa (sd 20 MPa).

The fatigue tests were performed at *R*=0.1 (frequency of 17 Hz) and at *R*=-1 (frequency of 11 Hz) in load control, in this latter case the mechanical frequency was lower to avoid an excessive temperature increasing.

Two different incremental stress blocks sequences (one for the tests of each stress ratio) were adopted for performing stepwise loading tests. Each block foresees the application of a fixed stress amplitude and mean stress for 20,000 cycles. The loading sequence runs up to the material failure.

The *UTS* value was useful to establish the maximum load of each block of the test sequence. As described in previous works [21,24,31,32], the maximum stresses of the initial loading blocks were less than the 50% of *UTS*. In effect the applied loadings for the tests at R=-1 ranged between 25-61%UTS while at R=0.1 the loadings ranged between 30-91%UTS.

During fatigue tests, the thermal signal was acquired by using the FLIR X6540sc cooled infrared detector with In-Sb sensor and windowing of 640x512. The detector was positioned in front of the sample, Fig. 2(b), and the millimetre-to-pixel ratio was of 0.25. The thermographic sequences were acquired for 10 seconds at 175 Hz (tests at R=0.1) and 123 Hz (tests at R=-1), the used integration time was 0.97 milliseconds while the used temperature interval was 10-90 °C (tests at R=0.1) and 10-90 °C; 80-200 °C (tests at R=-1).

Each infrared sequence acquisition corresponded to respectively 170 and 110 mechanical loading cycles imposed to samples.

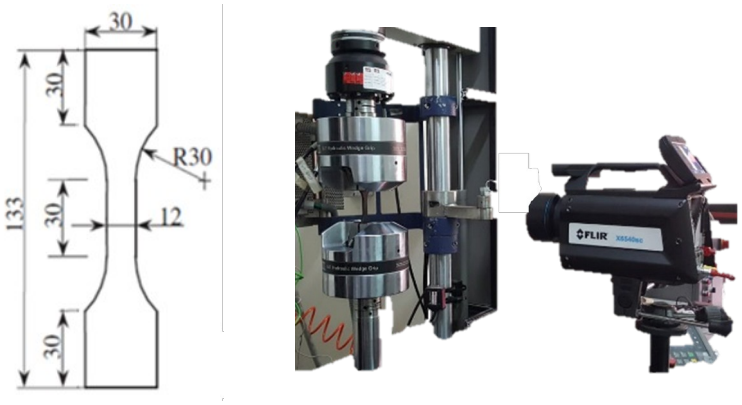

(a) (b)

Figure 2. (a) Sample geometry and (b) experimental set-up

2.2. Acquisition strategy: correlation between thermal and mechanical acquired data

Thermal acquisitions of each loading block (20,000 cycles in total) were performed in correspondence of 5,000-10,000-15,000 cycles. This allowed us to study damage evolution during the loading cycles.

Obviously, a correlation between the data in terms of stress, strain and time and the thermal data was performed with the aim to analyse the same data for a specific time instant.

Fig. 3 shows both mechanical data in terms of hysteresis loops (vectors of stress, strain and time acquired) and thermal data in terms of signal maps during loading cycles of a single loading block carried out at fixed σ_a. The region of interest corresponds to the gauge length area between the clips of the extensometer.

Substep 1 corresponded to the data acquired between 5,000 and 5,170 cycles (5,000-5,110 cycles, at *R=-1*) while Substep 2 corresponded to the data between 10,000 and 10,170 cycles (10,000-10,110 cycles, at *R=-1*). Substep 3 corresponded to the data between 15,000-15,170 cycles (15,000-15,110 cycles, at *R=-1*). As represented in Fig. 3 the analysed mechanical and thermographic data

correspond to the same time instant (loading cycles) and they have been acquired for the same duration (Substep).

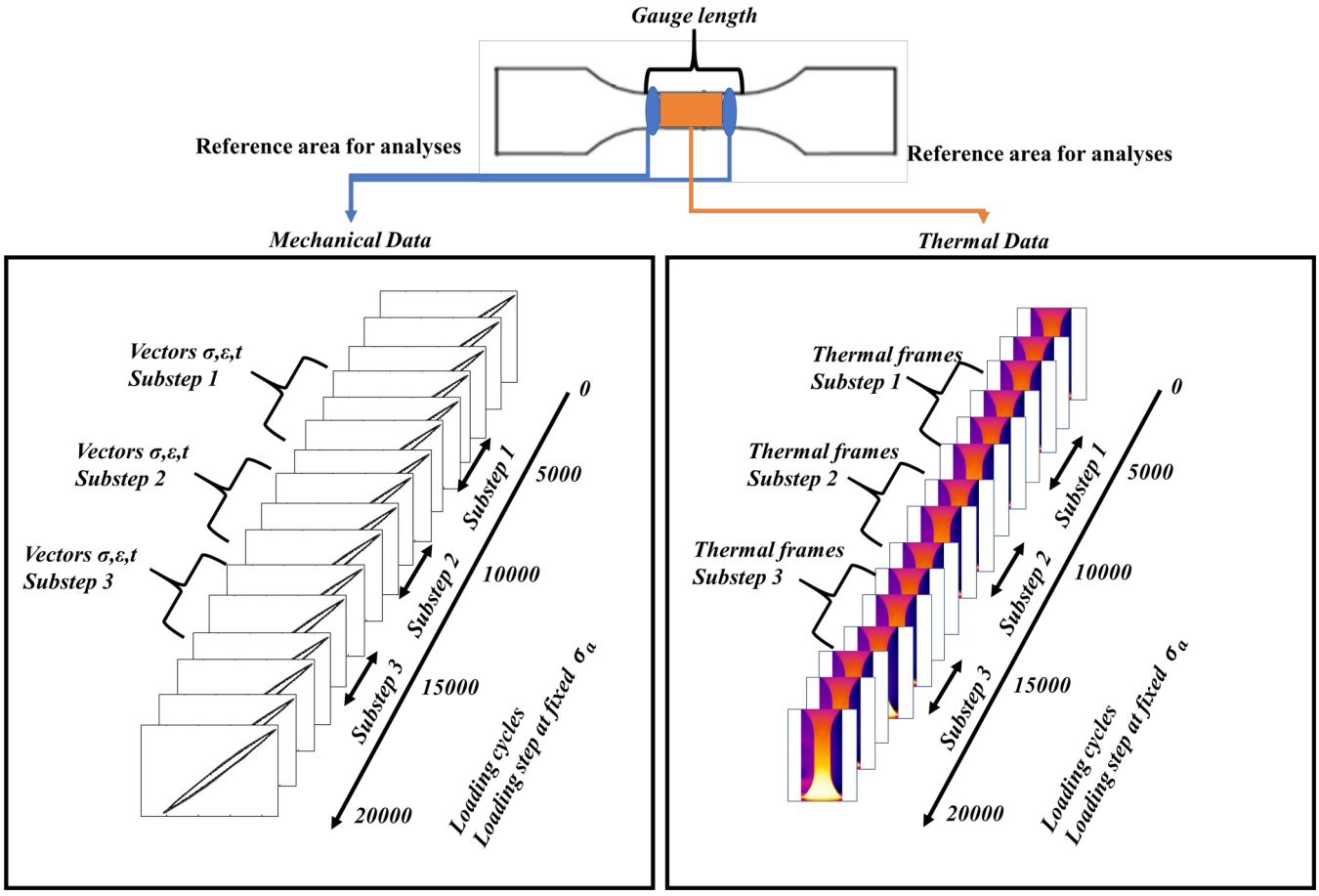

Figure 3. Strategy of data acquisitions and quantities acquired.

2.3. Data adopted for synthetic analysis of $\dot{W}$ and *Wp*

The mechanical energy rate $\dot{W}$ according to the model of Eq. 5, have been also analytically evaluated with the aim of understanding the energy distribution among the components of the frequency spectrum, such that can be considered as a guideline to understand mechanical data. To this purpose two stress levels in terms of σ_a have been selected: 147 MPa and 258 MPa for the test at *R=0.1* and 230 MPa and 320 MPa for the test at *R=-1*. The first stress level of each couple represents an initial stress level where damage is supposed to be absent or negligible and the second is where damage is significant.

The input parameters introduced in the model to evaluate $\dot{W}$ are reported in the following Table I:

Table I. Input parameters for synthetic data

Loading	Substep	R	ε_m [mm/	ε_a	σ_m	σ_a	φ [rad]

block			mm]	[mm/mm]	[MPa]	[MPa]	
n. 3	1	0.1	0.0040	0.0007	176	147	$\pi/1000$
	2		0.0040	0.0007	176	147	$\pi/1000$
	3		0.0040	0.0007	176	147	$\pi/1000$
n. 13	1	0.1	0.0280	0.0123	316	258	$\pi/50$
	2		0.0290	0.0123	316	258	$\pi/50$
	3		0.0300	0.0123	316	258	$\pi/50$
n. 3	1	-1	0.0002	0.0011	0	230	$\pi/800$
	2		0.0002	0.0011	0	230	$\pi/800$
	3		0.0003	0.0011	0	230	$\pi/800$
n. 10	1	-1	0.0004	0.0015	0	320	$\pi/70$
	2		0.0005	0.0015	0	320	$\pi/45$
	3		0.0006	0.0015	0	320	$\pi/35$

The strain, $\varepsilon_{m,}\varepsilon_a$ values were selected close to the measured experimental data. A ratcheting on ε_m was assumed toward the cycles of three substeps depending on imposed mean stress [8] and becoming significant at higher imposed stress levels. The parameter φ was assumed constant in each load step and through the substep, except for the second stress level at R=-1, where due to high intrinsic dissipations, it cannot be assumed constant.

The time vector used for the analysis was built in function of the sampling frequency (f_c) of mechanical data (204 Hz) and the period ($1/f_c$) which determines the step increment of the vector between the initial/final time of each substep.

4. Methods and data processing

In the present section, the overall methodologies used for analyses of both the mechanical and thermographic data are presented.

Fig. 4 resumes the workflow of the activity. The SAH of heat dissipated energy rate has been evaluated through the assessment of $\Delta T_{2\omega}$ component, and then correlated to the corresponding SAH of mechanical energy rate $\Delta \dot{W}_{2\omega}$to investigate the dependence and to assess the coefficients of the model function f¿).

The same experimental data measured by extensometer and used for evaluating $\dot{W}$ were adopted to estimate the area under the hysteresis loop (W_p).

In the following paragraphs the methodologies will be explained more in detail.

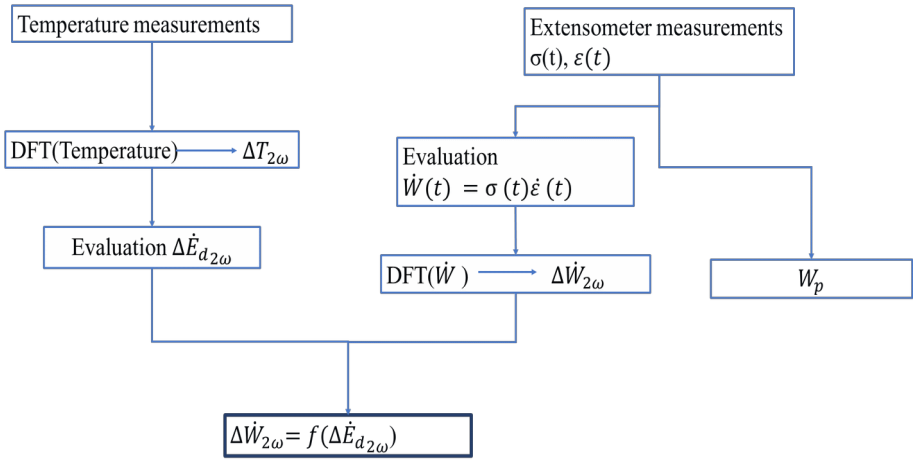

Figure 4. Workflow of the performed analysis and investigated relations.

4.1. Mechanical data

The data acquired by the extensometer are in the present section processed to obtain the mechanical energy rate function $\dot{W}$. The data output is represented by stress (σ), strain (ε) and time (t) vectors. The following list (according to Fig. 4) reports the detailed analysis carried out to obtain $\Delta \dot{W}_{2\omega}$ via the assessment of $\dot{W}$:

1. Assessing the vectors of σ and ε.
2. Evaluating $\dot{\varepsilon} = \Delta\varepsilon / \Delta t$, the approximate time derivative of the strain by using the Matlab operator 'diff' that calculates finite differences between adjacent elements of a vector along a specific array dimension.
3. Evaluating $\dot{W}$ as the product between σ and $\dot{\varepsilon}$.
4. Performing the Discrete Fourier Transform (DFT) of $\dot{W}$ by using a specific algorithm [43] based on Matlab fast Fourier transform tool.
5. Assessing the SAH of mechanical energy rate, $\Delta \dot{W}_{2\omega}$.

$\dot{W}$ has been also evaluated analytically by using the stress-strain constitutive law approach, Eq. 5. From the frequency spectrum of $\dot{W}$ it is possible to extract the synthetic peak to peak amplitude of the second harmonic, $\Delta \dot{W}_{2\omega}$.

The data processing to estimate the area under the hysteresis loop is based on the procedure presented in [42]. In particular, for each time instant the coupled values of the vector σ and ε, were evaluated computing the approximate integral of the vectors via the trapezoidal method with unit spacing. To perform the numerical integration on discrete data sets with $N+1$ evenly spaced point, the approximation is provided by the following formula:

$$W_p = \int_{\varepsilon_m}^{\varepsilon_M} \sigma d\varepsilon \approx \frac{\varepsilon_M - \varepsilon_m}{2N} \sum_{n=1}^{N} \left(\sigma\left(\varepsilon_n\right) + \sigma\left(\varepsilon_{n+1}\right) \right) \tag{14}$$

where ε_M and ε_m are respectively the maximum and minimum strain of the vector ε.

4.2. Thermal data

The processing of thermal data involved the following stages:

1. Acquisition of the temperature signal, *T(t),* from infrared thermal camera.
2. Selection of a region of interest (ROI) whose data (temperature over the time) are exported.
3. Evaluation of the mean value *($T_m(t)$)* of the ROI in each frame of the temporal sequence.
4. Performing the Discrete Fourier Transform (*DFT*) of the temperature signal by using a specific algorithm [43] based on Matlab® fast Fourier transform tool.
5. Assessing the SAH of temperature signal, $\Delta T_{2\omega}$.
6. Evaluating SAH of heat energy rate dissipated $\Delta \dot{E}_{d2\omega}$ by using Eq. 13 .

5. RESULTS

In present section, the results for the tests carried out at R=-1 and R=0.1 in terms of $\Delta T_{2\omega}$, $\Delta \dot{E}_{d2\omega}$, $\Delta \dot{W}_{2\omega}$,W_p.

5.1. Hysteresis loops: qualitative and quantitative assessment

The hysteresis loops (through 170 cycles) are reported for the stepwise tests at *R*=0.1, Fig. 5 (a) at σ_a= 147 MPa and Fig. 5 (b) at σ_a= 258.3 MPa, for the sample S_1. Synthetic data ($S_{1\,sim}$) and measured data ($S_{1\,exp}$) are reported with the same colour line for each sub-step.

The hysteresis loops in Fig. 5(a) are stretched while they become wider at a higher applied stress level and after the specific loading history provided by stepwise loading (Fig. 5(b)), while the ratcheting is present and it becomes important at higher imposed mean stresses. Moreover, the Young's modulus variation can be also observed from the first to the last test as further sentinel of the ongoing damage.

The model adopted for simulating synthetic data, runs quite well at higher imposed stress levels (no difference between $S_{1\,sim}$ and $S_{1\,exp}$ in Fig. 5(b)) while it has some difficulties to represent the data at lower applied stresses (quite significant data scatter between $S_{1\,sim}$ and $S_{1\,exp}$ in Fig. 5(a)). This can be explained by considering that when the load is in pure elastic range it is difficult to fit the data by using a visco-elastic model.

The hysteresis loops (110 cycles) for the S_1 of test at *R=-1* are reported in Fig. 5: (c) at σ_a= 230 MPa and (d) at σ_a=320 MPa. They are stretched at lower imposed stresses while they become wider at a higher applied stress level. The ratcheting is less accentuated than the ratcheting behaviour of previous Fig. 5(a)-(b) due to zero mean stress. The Young's modulus variation can be observed between the curves of the test at σ_a=320 MPa.

Even in this case the model adopted for simulating hysteresis loops runs quite well at higher imposed stress levels (very small scatter between $S_{1\ sim}$ and $S_{1\ exp}$ in Fig. 5 (d) while it has some difficult to fit the data at lower applied stresses as the cycle approximates a straight line (cycle flattened).

A general consideration observing Fig. 5 is such that the hysteresis loops are wider in the case of the tests at *R=-1* clearly due to a higher energy dissipation.

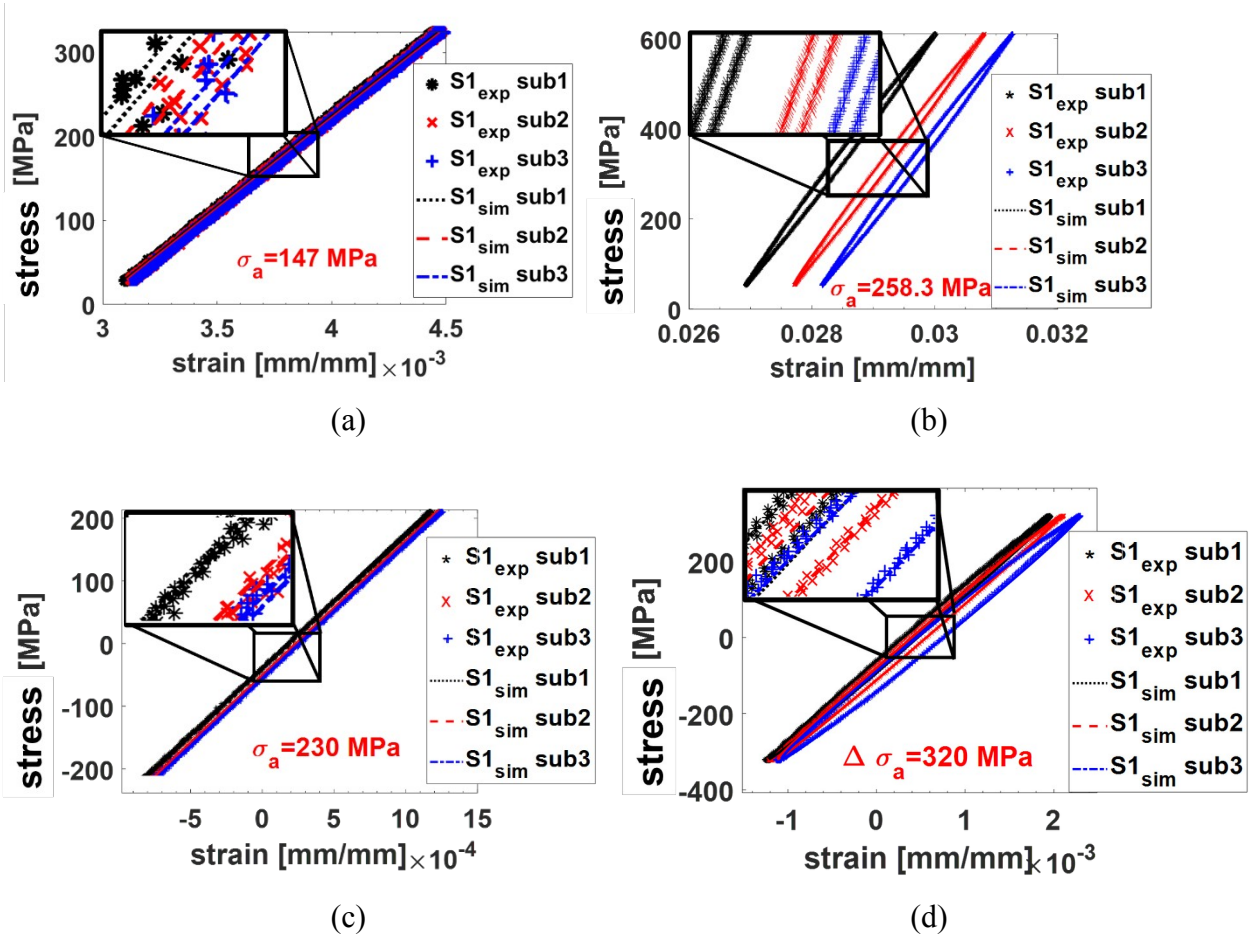

Figure 5. Hysteresis loops measured and simulated at R=0.1: (a) σ_a=147 MPa and (b) σ_a=258 MPa and R=-1 (c) σ_a=230 MPa and (d) σ_a=320 MPa

The curves reported in Fig. 6 show for the S_1 of the series at *R=0.1* and *R=-1*, the hysteresis loops corresponding to one cycle acquired in the substep 2 at each imposed stress level.

The coupling effect of increasing imposed amplitude and mean stress determines a shift of the curves that is more accentuate for the tests at *R*=0.1, Fig. 6(a). It is interesting to observe the significant variation in terms of strains between hysteresis loops at 200 MPa and those at 217 MPa, also present in the curves at *R*=-1 (Fig. 6(b)) between σ_a=290 MPa and σ_a=300 MPa, even if it is less pronounced. These differences in the behaviours at both stress ratios can be explained by

considering that changes in the regime of damage accumulation occurs depending on the stress ratio. In the work of Nourian-Avval [23] that point corresponded to the inelasticity point transition where a change in the mechanisms of strains occurs, and above it the permanent movement of the dislocations determines an unrecoverable deformation status of the material [44-46].

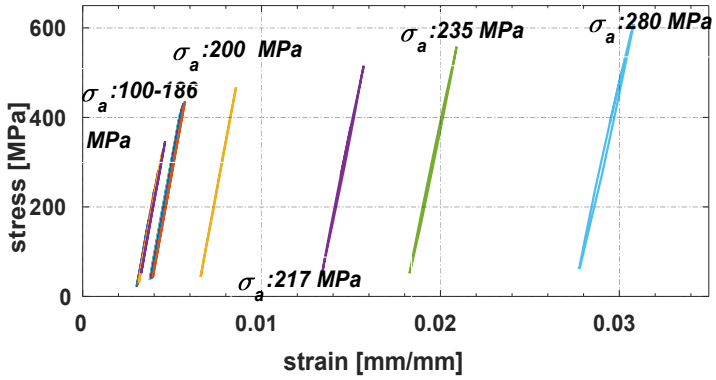

(a)

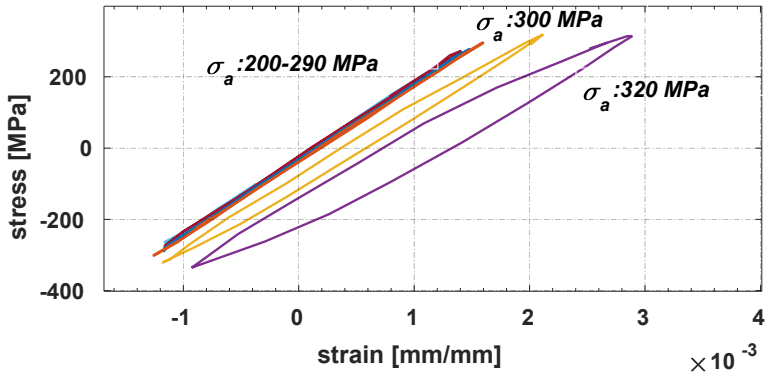

(b)

Figure 6. Hysteresis loop of a stepwise test for samples S_1 tested at R=0.1 and R=-1.

5.2. Mechanical energy rate $\dot{W}$ and components of the frequency spectrum

In present section, the $\dot{W}$ values of S_1 are presented at a specific imposed stress level: σ_a= 258.3 MPa for R=0.1 and σ_a= 320 MPa for R=-1.

Fig. 7(a) reports $\dot{W}$ over ten cycles (0.588 s) where synthetic data are superimposed on those measured. The synthetic and measured spectra, Fig. 7(b)-(c), in terms of amplitudes are similar. This confirms the goodness of the adopted simple visco-elastic model in reproducing experimental data. It is interesting to observe that the presence of the mean stress in the imposed loads determines an hump in the $\dot{W}$ function and the energy is divided into two major contributions: the first at 17 Hz and the second at 34 Hz, twice of the loading frequency.

In Fig. 8, the $\dot{W}$ values over ten cycles (0.9 s) are presented for sample S_1 tested at R=-1. In this case, the there is a little difference between synthetic and measured data due to data sampling, however it is evident that the fundamental frequency of the $\dot{W}$ spectrum is 22 Hz (twice the loading frequency of 11 Hz). As previously said, the mean stress effect on mechanical energy rate acts by shifting fundamental angular frequency from 2ω to 1ω. Fig. 8(b)-(c), in terms of amplitudes are similar.

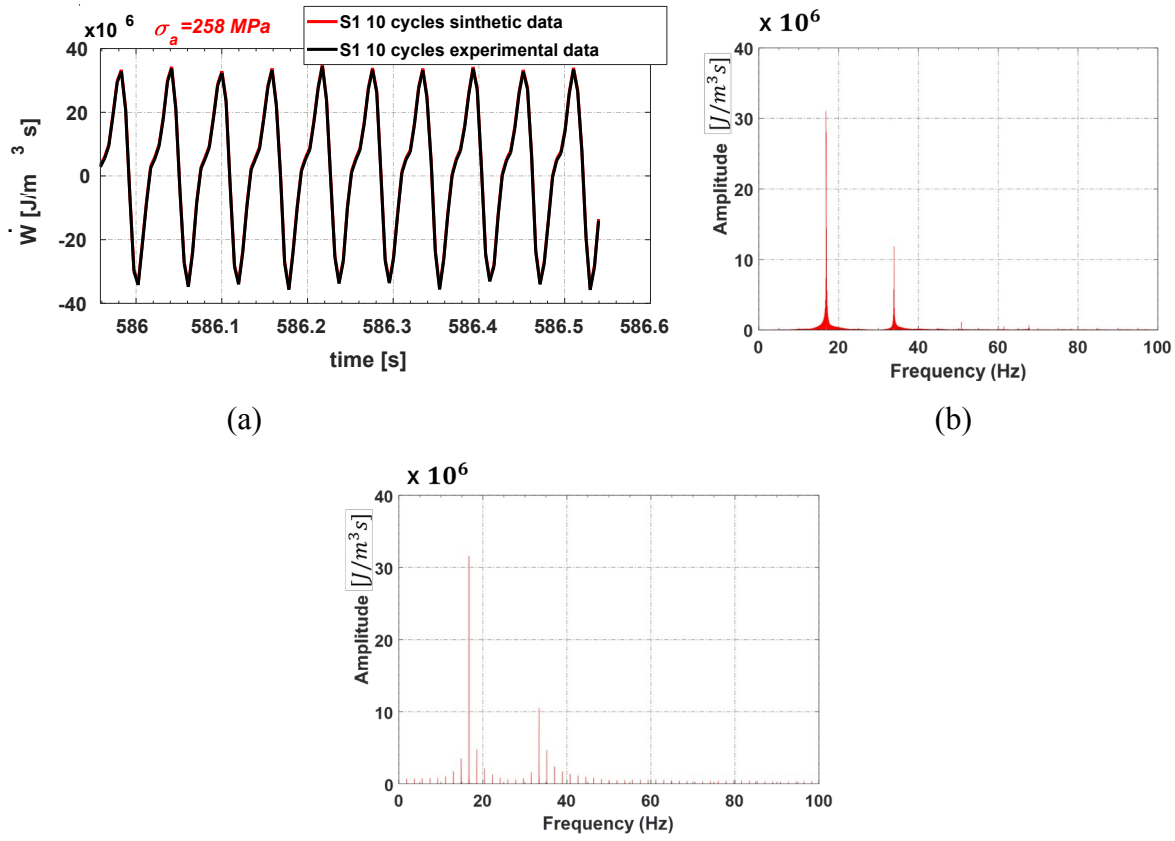

(a) (b)

(c)

Figure 7. (a) $\dot{W}$ for S_1 tested at R=0.1 (simulated and experimental), spectrum of $\dot{W}$ (b) experimental and (c) simulated.

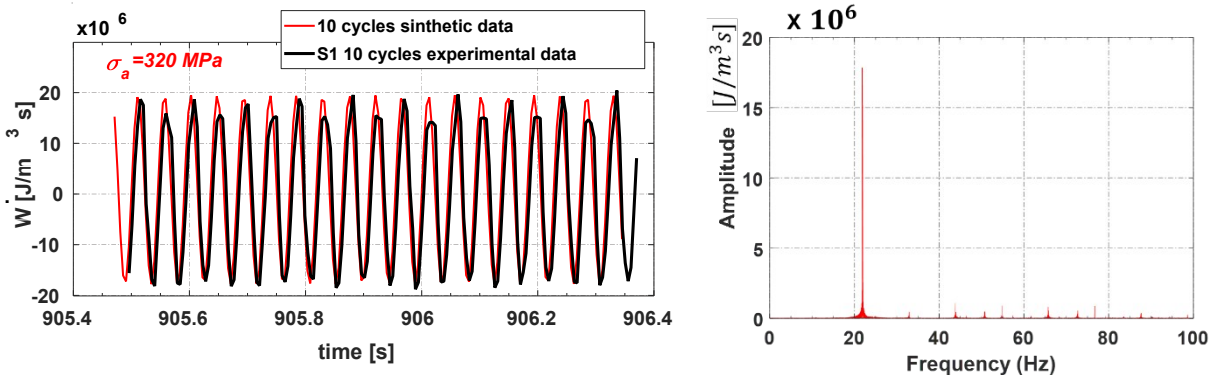

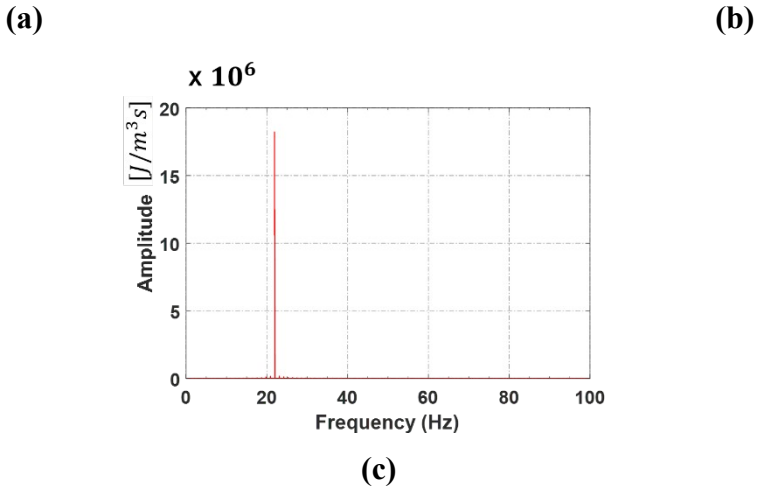

Figure 8. (a) $\dot{W}$ for S_1 tested at R=-1 (simulated and experimental), spectrum of $\dot{W}$ (b) experimental and (c) simulated.

Another way to observe the difference at two stress ratios in harmonic energy distribution for the tested samples is provided by Fig. 9 where, the experimental data are presented in terms of $\Delta\dot{W}$, and $\Delta\dot{W}_{2\omega}$. One can firstly note that the total amount of energy supplied to the material is totally ascribed to SAH for those tests at R=-1(whited diamond markers, R^2=0.98) while at R=0.1 the energy contribution of $\Delta\dot{W}_{2\omega}$, is fifth times lower than $\Delta\dot{W}$ as demonstrated by frequency spectra previously reported.

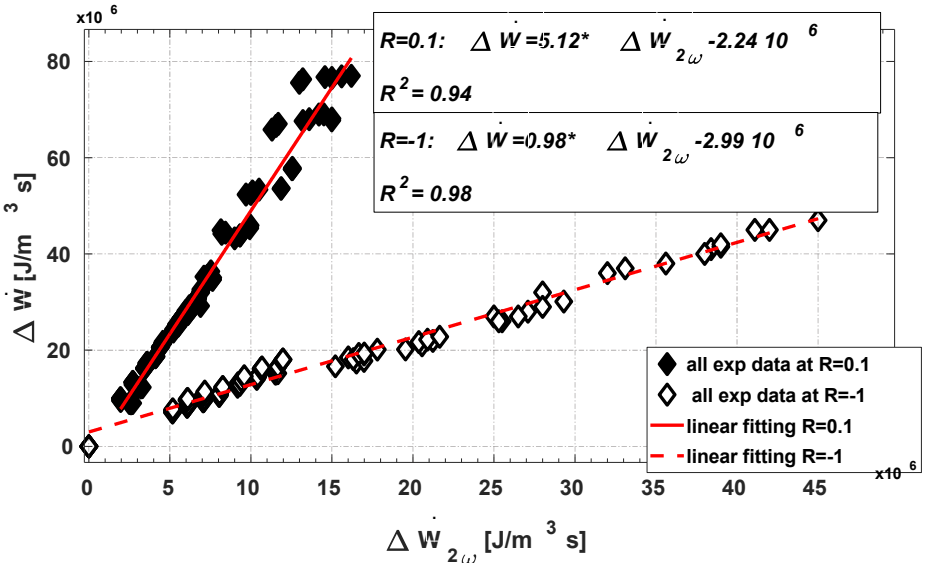

Figure 9. Relation between $\Delta\dot{W}$ and $\Delta\dot{W}_{2\omega}$

The $\Delta \dot{W}_{2\omega}$ curves of overall samples (and related measured values in the sub-steps) are presented for the *R=0.1* (Fig.10 (a)) and *R=-1* (Fig. 10 (b)) where the SAH values are higher due to higher intrinsic energy dissipations.

In Fig.10(a), the increase of $\Delta \dot{W}_{2\omega}$ during the test for all the samples is continuous, even if a small slope changing few stress levels before 200 MPa can be observed. At *R=-1*, Fig.10(b), $\Delta \dot{W}_{2\omega}$ data presents a marked slope variation in correspondence of 300 MPa due to inelastic point transition [23,44-46].

In general, a major data dispersion is observed for the points above 200 MPa and points above 300 MPa, more accentuated for the data of Fig.10(b)due to highest energies involved for the material damaging but a good reproducibility of the results is evident.

The $\Delta \dot{W}_{2\omega}$ behaviour at two stress ratios is presented versus the loading cycles in Fig.10(c)-(d). The rectangular blocks represent the data of the substep for each imposed stress level.

For the test results at *R=0.1* a double slope change is observable after 136 MPa and 200 MPa(Fig. 10(c)) and in general for each sample the $\Delta \dot{W}_{2\omega}$increase through the substep is evident just after 200 MPa. Before this point the $\Delta \dot{W}_{2\omega}$ variation in the loading step is roughly zero. The same behaviour is observed in Fig. 10(d) for the $\Delta \dot{W}_{2\omega}$ values at *R=-1* around the inelastic point of 300 MPa.

In addition, the ratcheting in $\Delta \dot{W}_{2\omega}$is absent before the inelastic point transition where the signal stabilisation is present. As a consequence, it is possible to conclude that the signal stabilisation does not occur in presence of accumulated damage and then a careful attention must be paid in the evaluation of energy-based parameters for fatigue damage investigations.

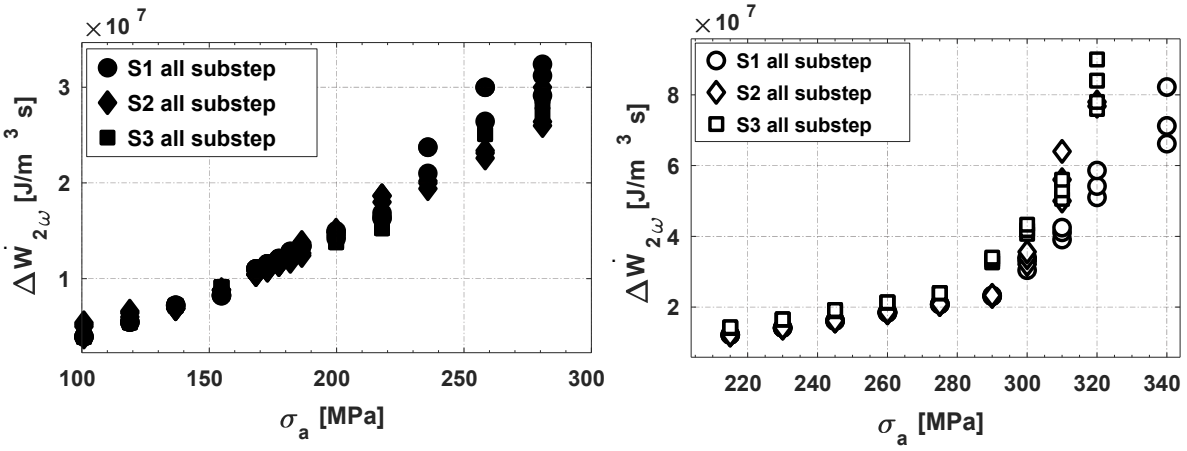

(a) **(b)**

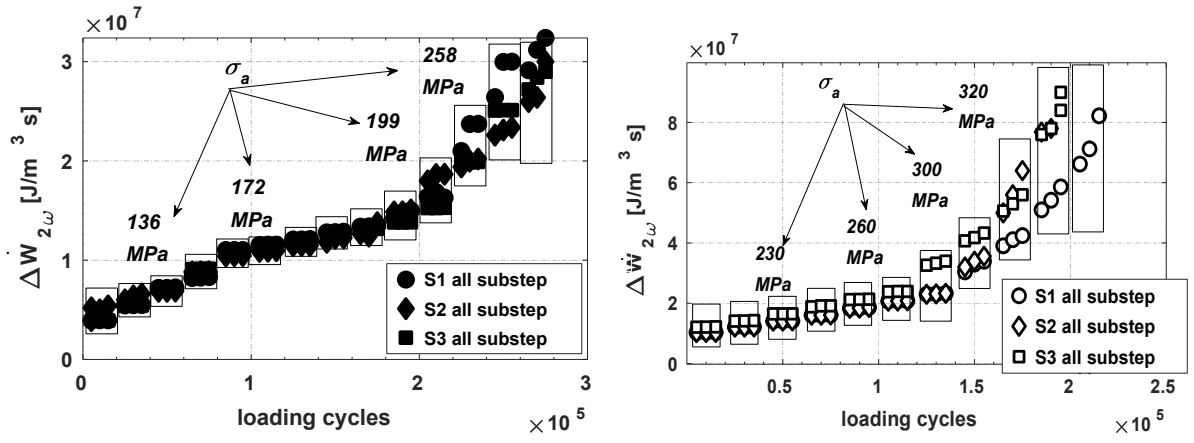

Figure 10. $\Delta \dot{W}_{2\omega}$ assessed for each imposed σ_a: (a) R=0.1 and (b) R=-1 and evolution through cycles: (c) R=0.1 and (d) R=-1.

5.3. Thermal data analysis: from temperature to heat dissipated energy rate

The curves of $\Delta T_{2\omega}$ for each sample and related sub-step at *R=0.1* (Fig. 11(a)) and *R=-1* (Fig. 11(b)) are reported. The Fig. also show the spectra of the temperature signal and a focus on SAH. In both cases, the fundamental component is at the loading frequency (respectively 17 Hz and 11 Hz for the data of Fig. 11 (a)-(b)) while the SAH component is lower. This can be explained by considering the effect of thermoelastic temperature variations added to the signal from dissipative temperature variations [38].

By observing Fig.11(a), it is evident a good reproducibility of the tests and a little data scatter especially at higher imposed stress levels. The curves also present a continuous increase with a slight slope change between 150- 200 MPa. The same good reproducibility of the tests can be found for the test at *R=-1*, Fig.11(b), while a major data scatter is observed in the data points after the inelasticity point transition, in good agreement with mechanical data behaviour.

The higher $\Delta T_{2\omega}$ values at *R*=-1 than at *R=0.1* can be explained by the major intrinsic dissipations in agreement with the results presented in literature [19,32].

In Fig. 12(a)-(b), the parameter $\Delta \dot{E}_{d2\omega}$ is represented respectively versus stress amplitude and the loading cycles. $\Delta \dot{E}_{d2\omega}$ data reflects those of $\Delta T_{2\omega}$, Fig.11(a)-(b). As for Fig.12 (c)-(d), it is possible to observe that the $\Delta \dot{E}_{d2\omega}$ trend is the same of $\Delta \dot{W}_{2\omega}$ (Fig. 10(c)) presenting two slope variations in correspondence of the same loading cycles, and it is interesting to highlight the great correlation between the two quantities. The same consideration can be drawn for the $\Delta \dot{E}_{d2\omega}$ of Fig. 12(d) in agreement with those of $\Delta \dot{W}_{2\omega}$ (Fig. 10(d)), however in this case the slope variation of $\Delta \dot{W}_{2\omega}$ at 150,000.0 cycles is less marked in $\Delta \dot{E}_{d2\omega}$. It is possible also to note that thermal parameter is very

sensitive to loading history (more than $\Delta \dot{W}_{2\omega}$), in effect, even at low imposed stresses it is difficult to assume that thermal signal stabilises.

The values of $\Delta \dot{E}_{d2\omega}$ are clearly smaller than $\Delta \dot{W}_{2\omega}$ as they represent an estimation of the heat dissipated energy rate.

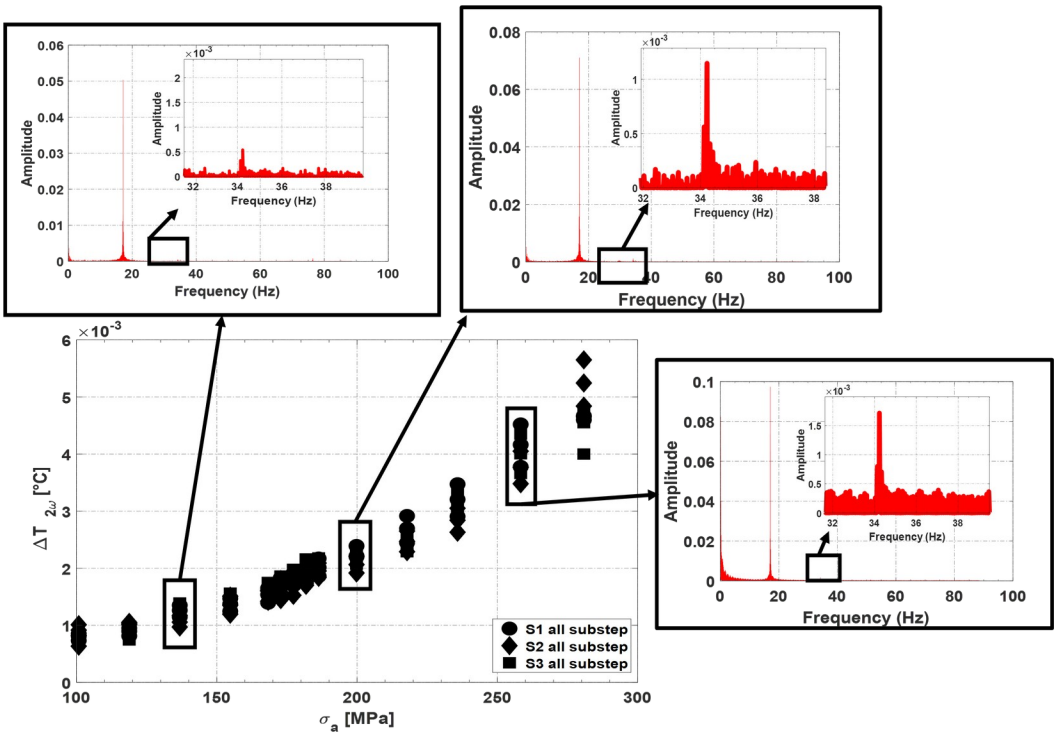

(a)

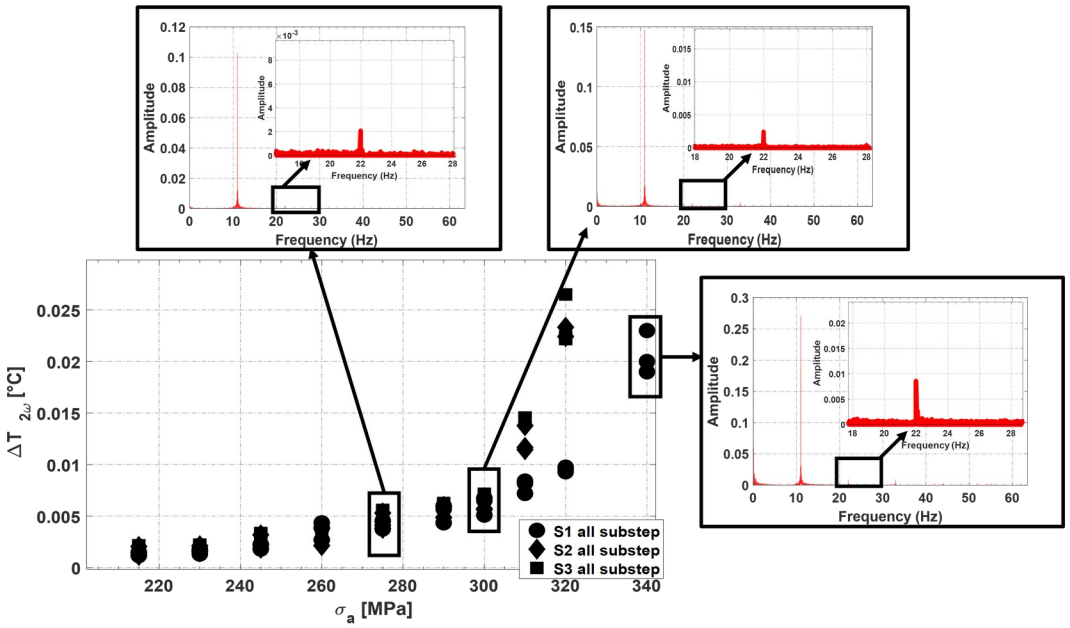

(b)

Figure 11. $\Delta T_{2\omega}$ at (a) R=0.1 and (b) R=-1.

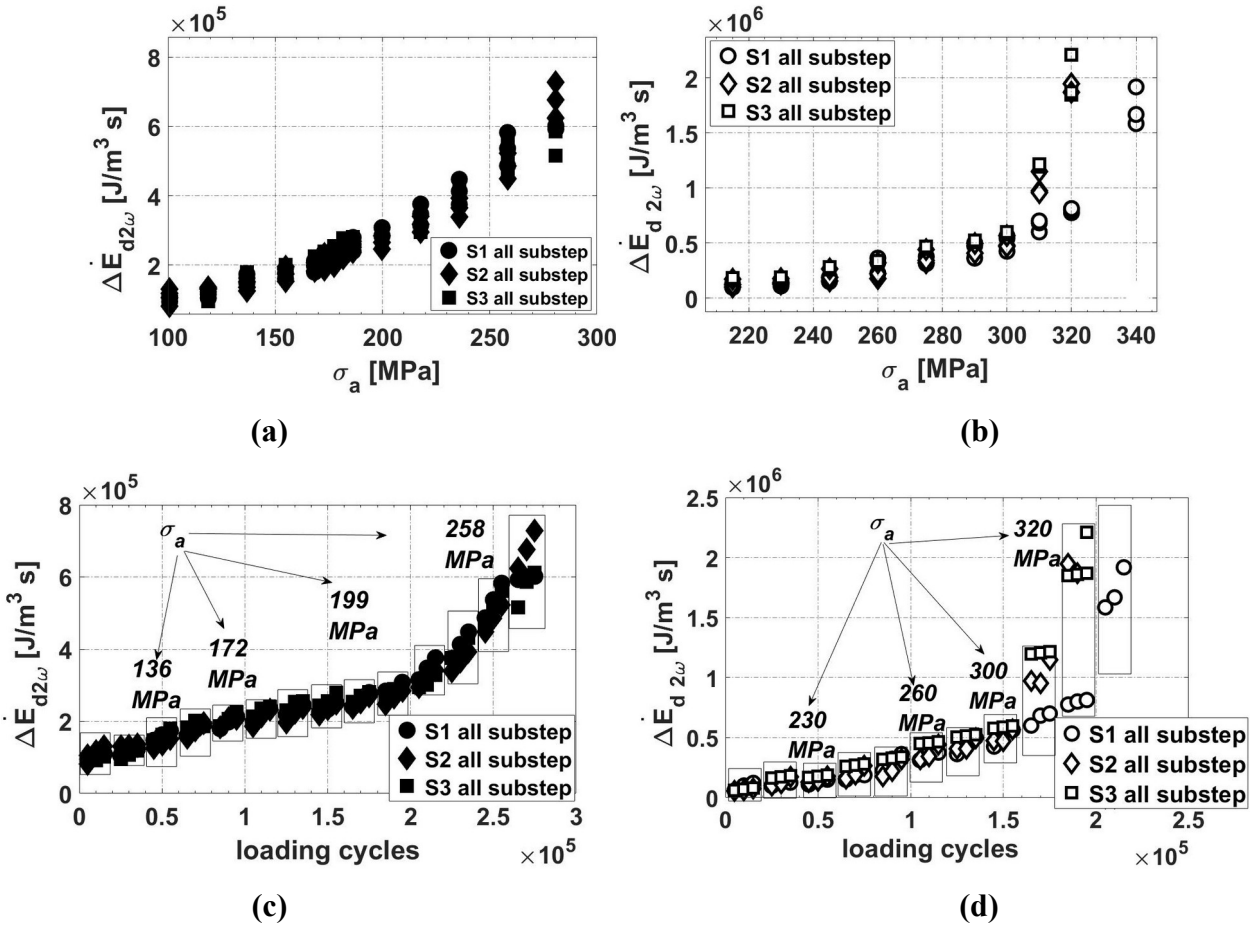

Figure 12. $\Delta \dot{E}_{d2\omega}$ assessed at (a) R=0.1 and (b) R=-1 and through the cycles at (c) R=0.1 and (d) R=-1.

6. Discussion:

6.1. Investigation on the relationship between $\Delta \dot{E}_{d2\omega}$ and $\Delta \dot{W}_{2\omega}$

In present section, finally the relation between $\Delta \dot{E}_{d2\omega}$ and $\Delta \dot{W}_{2\omega}$ has been here investigated for each sample of the tests at *R=0.1* and *R=-1*.

In Fig. 13(a) for *S1 R=0.1* one can observe a linear correlation between $\Delta \dot{E}_{d2\omega}$ and $\Delta \dot{W}_{2\omega}$ with high R^2 coefficient with all the data that lying within the prediction bounds defined with a 95% level of confidence. These bounds measure the confidence that the new observation lies within the interval given by a single predictor value.

The same kind of data for the test at *R=-1* in Fig. 13(b), show a linear relationship between $\Delta \dot{E}_{d2\omega}$ and $\Delta \dot{W}_{2\omega}$ with a quite wider scatter due to the less number of acquired thermal data.

For overall data of the two experimental campaign the relationship between $\Delta \dot{E}_{d2\omega}$ and $\Delta \dot{W}_{2\omega}$ has been investigated, Fig. 13(c). It is very important to observe as all the data can be approximated with a high coefficient of determination by the unique linear relationship that does not depend on

damage accumulation mechanisms and cycles. The following formula describe the linear relation between $\Delta \dot{E}_{d2\omega}$ and $\Delta \dot{W}_{2\omega}$:

$$\Delta \dot{W}_{2\omega} = A_1 \Delta \dot{E}_{d2\omega} + A_2 \quad (15)$$

where the coefficients A_1, A_2 depend on material. The first is dimensionless while the A_2 dimension is the same of $\Delta \dot{E}_{d2\omega}$ and $\Delta \dot{W}_{2\omega}$. The values of coefficients and related statistics for all the tested samples are reported in Table II.

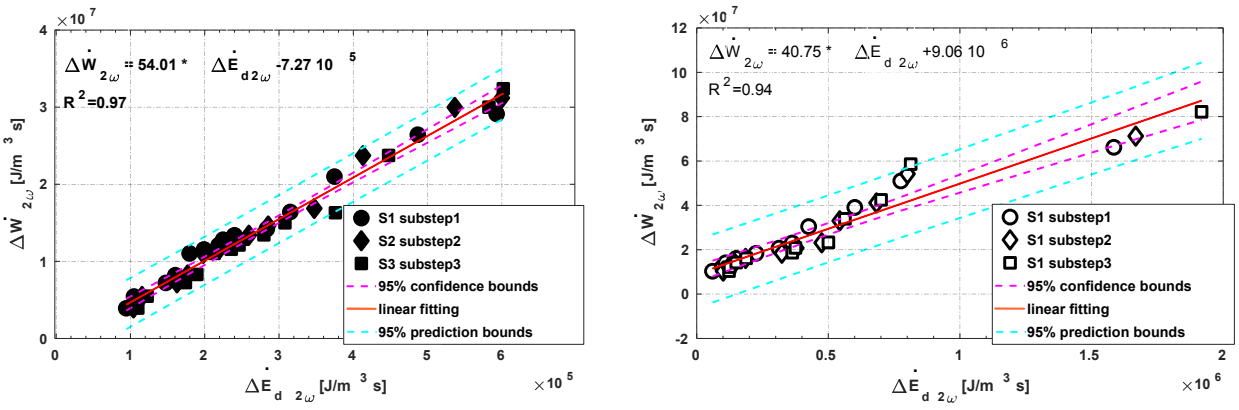

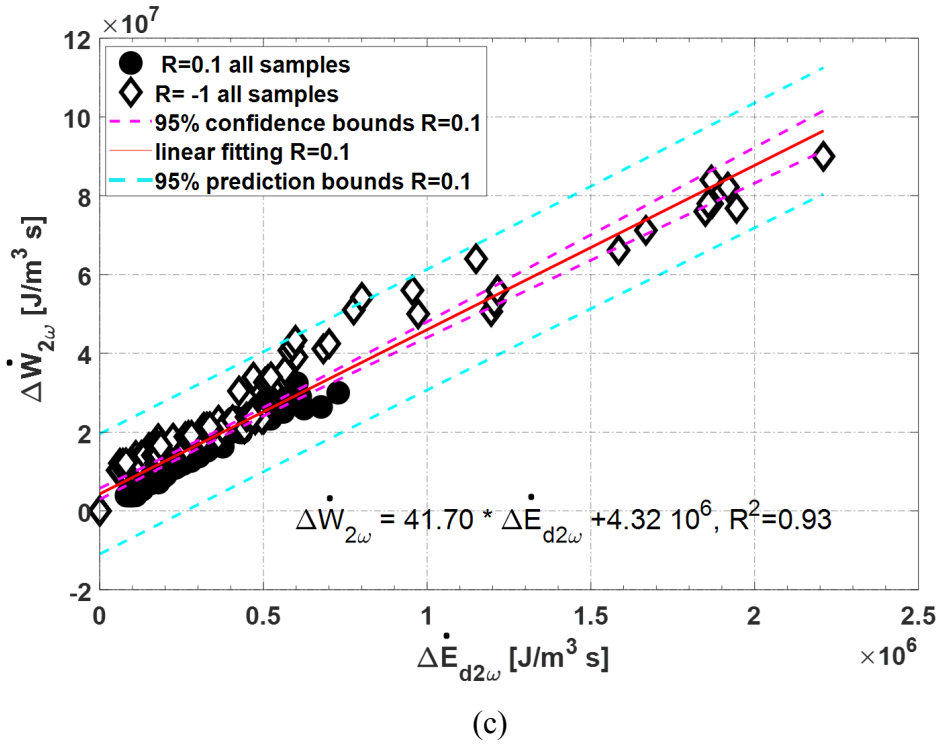

Figure 13. Relation between $\Delta \dot{E}_{d2\omega}$ and $\Delta \dot{W}_{2\omega}$ for S_1 tested at (a) R=0.1 (b) R=-1, and (c) overall data for the six samples tests at R=0.1 and R=-1.

Table II. Coefficients A_1 A_2 with 95% confidence bounds (lower/upper) on coefficients of linear model

Samples tested at R=0.1		
Sample	A_1**[ad]**	A_2 **[J/m^{3}s]**
1	54.01±2.45	-7.27 10^5±7.73 10^5
2	41.27±3.55	+2.32 10^6 ± 1.10 10^6
3	48.86±2.13	-1.86 10^4± 6.55 10^5
Samples tested at R=-1		
Sample	A_1**[ad]**	A_2 **[J/m^{3}s]**
1	40.75±4.25	+9.06 10^6± 2.82 10^6
2	39.03±2.98	+8.17 10^6± 2.21 10^6
3	38.86±3.13	+8.97 10^6± 2.34 10^6
Overall data		
Sample	A_1**[ad]**	A_2 **[J/m^{3}s]**
All tested samples	41.70±1.74	+4.32 10^6±9.10 10^5

6.2. SAH of the heat energy dissipated and area under the hysteresis loop

Under a quantitative point of view, the areas under the hysteresis loop measured for the samples tested at *R=0.1* and *R=-1* are presented in Fig. 14, compared to $\Delta E_{d2\omega}$ parameter. A slope change at a specific value of stress (approximately at 200 MPa, at *R=0.1* and at 300 MPa for the data at *R=-1*) characterises the data trends of both Fig. 14. This point according to the De Finis[43] corresponds to the endurance limit of the material. In addition, W_p and $\Delta E_{d2\omega}$ present the same behaviour in each case (*R=0.1* and *R=-1)* and for any test, and then it is possible to conclude that $\Delta E_{d2\omega}$ can be used to estimate the heat dissipated energy and then the area under the hysteresis loop. $\Delta E_{d2\omega}$ values are clearly lower than those of W_p as it represents just a portion of the heat converted energy.

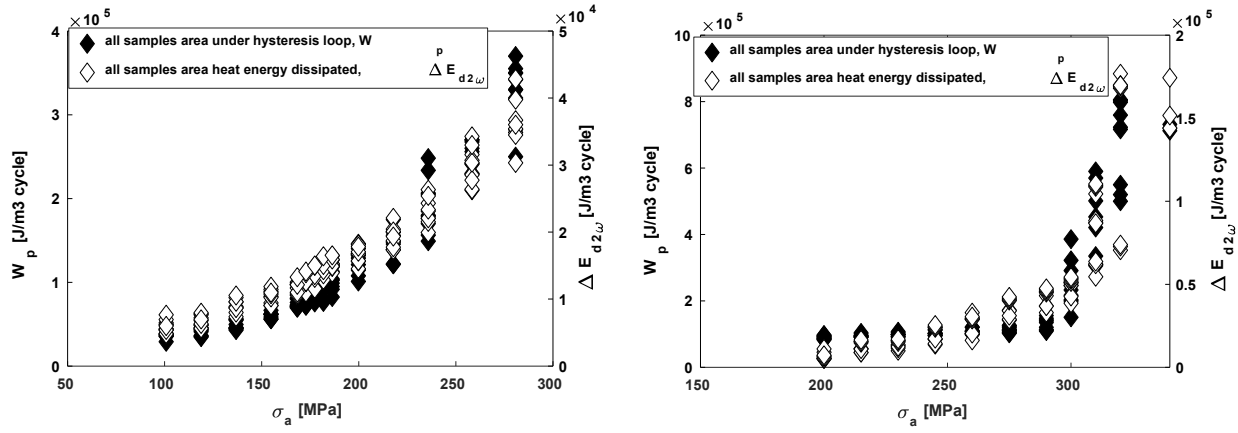

Figure 14. W_p and $\Delta E_{d2\omega}$ at (a) *R*=0.1 and (b) *R*=-1.

Conclusions

In present research, six samples of C45 steel were fatigue tested by using a stepwise loading sequence at R=0.1 (three samples) and R=-1 (three samples). The rapid fatigue tests were assisted by an infrared detector and an extensometer.

The aim was first to study the harmonic energy rate distribution of both heat dissipated energy rate and mechanical energy rate. The experimental results show that in presence of the mean stress in the load, the mechanical energy spectrum is composed by different harmonic components (specifically in this case the first and second harmonics) while for a fully reversed load the fundamental component is the SAH. The heat dissipated energy presents a frequency spectrum composed by different harmonic components whatever the imposed stress ratio.

In addition, the relation between SAH of the heat dissipated energy rate and mechanical energy rate for different loading conditions has been investigated. The major outcome is such that the relationship between SAH of heat dissipated and mechanical energy rates depends only on material and does not depend on loading or damage level. The relationship is also valid, independently on signal stabilisation.

It was also investigated the capability of $\Delta T_{2\omega}$ for estimating the mechanical energy via the evaluation of the heat dissipated for different loading conditions. Even if, in presence of mean stress in the load, the SAH of the heat dissipated energy rate is not the only one related to the intrinsic dissipations, however it can be used to estimate $\dot{E}_d$ and then $\Delta \dot{W}_{2\omega}$.

The advantages of using the suggested procedure are:

- the material stabilisation (in terms of thermal signal) not required;
- the applicability of the procedure for any type of fatigue test and loading condition in terms of stress ratio since for the application of the method no assumptions are required on percentage of heat converted energy or any considerations on the shape (leaf, elliptical,..) or symmetry of hysteresis loop (the same material behaviour under tensile and compressive stress) are required;
- the possibility to perform a damage analysis as the SAH of temperature is strictly related to the dissipative heat sources and the applicability in those cases where mechanical data measurements are not feasible;

The potential of the adopted approach is such that it considers just the temperature variations related to dissipative phenomena so that the derived $\Delta \dot{E}_{d2\omega}$ is a good estimator of intrinsic dissipations.

Further development of the techniques will involve tests on component.

References

1. Feltner CE, Morrow JD. Microplastic Strain Hysteresis Energy as a Criterion for Fatigue Fracture. ASME Journal of Basic Engineering 1961;83:15-22.
2. Golos KM. Multiaxial fatigue criterion with mean stress Effect. Int. J. Pres. Vex & Piping 1996;69:263-266.
3. Morrow JD. Cyclic Plastic Strain Energy and Fatigue of Metals. Internal Friction, Damping, and Cyclic Plasticity, STP 378, American Society of Testing Materials1965,45-84.
4. Ellyn F, Kujawski D. Plastic Strain Energy in Fatigue Failure. J. Pressure Vessel Technol1984;106:343 .
5. Chiou YC, Yip MC. An energy−based damage parameter for the life prediction of AISI 304 stainless steel subjected to mean strain. Journal of the Chinese Institute of Engineers 2006;29:507-517.
6. Lazzarin P, Livieri P, Berto F, Zappalorto M. Local strain energy density and fatigue strength of welded joints under uniaxial and multiaxial loading. Eng Fract Mech 2008;1875–1889.
7. Koh SK. Fatigue damage evaluation of a high pressure tube steel using cyclic strain energy density. Int. J. Press. Vessels Pip 2002;79:791–798.
8. Golos K, Ellyn F. A Total Strain Energy Density Theory for Cumulative Fatigue Damage. J. Pressure Vessel Technol 1988;110:37.
9. Zarandi EP, Skallerud BH. Cyclic behavior and strain energy-based fatigue damage analysis of mooring chains high strength steel. Marine Structures 2020;70:102703.
10. Chang CS, Pimbley WT, Conway HD. An Analysis of Metal Fatigue Based on Hysteresis Energy. Exp Mech 1968;8:133-137.
11. Lachowicz CT. Calculation of the elastic–plastic strain energy density under cyclic and random loading. Int J Fatigue 2001;23:643–652.
12. Kliman V, Bily M. Hysteresis Energy of Cyclic Loading. Mater. Sci. Eng 1984; 68:11-18.
13. Bovsunovsky AP. Shape of a mechanical hysteresis loop for metallic materials under harmonic stresses below the fatigue limit. Part 1: Experimental method. Strength Mater 1997;29.
14. R. V. Lapshin, Analytical model for the approximation of hysteresis loop and its application to the scanning tunneling microscope. Rev Sci Instrum 1995;66:4718.
15. Frunză G, Diaconescu EN. Hysteresis and mechanical fatigue. The annals of university “dunărea de jos “ of galaţi fascicle VIII 2006 (XII), ISSN 1221-4590 Tribology.
16. Scott-Emuakpor1 O, George T, Cross C, Herman Shen MH. Hysteresis-loop representation for strain energy calculation and fatigue assessment. J. Strain Analysis 2010;45:275-282.
17. Letcher T, Auen C, Nesaei S, Nielsen M, Delfanian F. Hysteresis Strain Energy Behavior of Al6061-T6 With Multi-Fatigue Load Levels as Applied to an Energy-Based Fatigue Life Prediction Method. Proceedings of the ASME 2013 International Mechanical Engineering Congress and Exposition IMECE2013 November 15-21, 2013, San Diego, California, USA.
18. Lin YC, Chen XM, Liu ZH, Chen J. Investigation of uniaxial low-cycle fatigue failure behavior of hot-rolled AZ91 magnesium alloy. Int J Fatigue 2013; 48:122–132.

19. Crammond G, Boyd SW, Dulieu-Barton JM. Speckle pattern quality assessment for digital image correlation. Opt. Lasers Eng 2013;51:1368–1378.
20. La Rosa G, Lo Savio F, Giudice F, Clienti C, Marino Cugno Garrano A. Energetic analysis of fatigue hysteresis by thermographic and digital image correlation methodologies. Fatigue Fract Eng Mater Struct 2020;1–11.
21. Chrysochoos A, Berthel B, Latourte F, Galtier A, Pagano S, Wattrisse B. Local energy analysis of high-cycle fatigue using digital image correlation and infrared thermography. J. Strain Anal. Eng. Des 2008;43(6):411–422.
22. Munier R, Doudard C, Calloch S, Weber B. Determination of high cycle fatigue properties of a wide range of steel sheet grades from self-heating measurements. Int J Fatigue 2014;63:46–61.
23. Khonsari M, Amiri M. Introduction to thermodynamics of mechanical fatigue. CRC Press; 2012.
24. Nourian-Avval A, Khonsari MM. Rapid prediction of fatigue life based on thermodynamic entropy generation. Int. J Fatigue 2021;145:106105.
25. Luong MP. Infrared observation of thermomechanical couplings in solids. Thermosense XXIV conference, part of SPIE's Aerosense, 1−5 April 2002, Orlando (Florida).
26. Enke NF. An Enhanced Theory for Thermographic Stress Analysis of Isotropic Materials. Proc. SPIE 1084, Stress and Vibration: Recent Developments in Industrial Measurement and Analysis, (31 July 1989); doi: 10.1117/12.952908
27. Jordan EH. Temperature Based Stress Analysis of Notched Members. Ph.D. Thesis, Dept. of Engineering Mechanics, Univ. of Wisconsin- Madison, 1978.
28. Enke NF, Sandor BI. Cyclic Plasticity Analysis by Differential Infrared Thermography. Proc. Sixth International Congress on Experimental Mechanics, Portland, Oregon, June 1988, pp. 830 -835.
29. Biot MA. Thermoelasticity and Irreversible Thermodynamics. J. Appl. Phys 1956;27:240 -253.
30. Sakagami T, Kubo S, Tamura E, Nishimura T. Identification of plastic−zone based on double frequency lock−in thermographic temperature measurement. International conference of fracture ICF11 2015, Catania (Italy)
31. Krapez JK, Pacou D, Gardette G. Lock−in thermography and fatigue limit of metals. Quantitative infrared thermography, QIRT, 18−21 July 2000. Reims (France).Noi
32. De Finis, R., Palumbo, D., Ancona, F., Galietti, U. Fatigue limit evaluation of various martensitic stainless steels with new robust thermographic data analysis. Int. J. Fatigue 2015;74:88–96.
33. De Finis R, Palumbo D, Galietti U. A multianalysis thermography-based approach for fatigue and damage investigations of ASTM A182 F6NM steel at two stress ratios. Fat. Fract. Eng Mat Struct 2019;42(1):267–283.
34. De Finis R, Palumbo D. Estimation of the dissipative heat sources related to the total energy input of a cfrp composite by using the second amplitude harmonic of the thermal signal. Materials 2020;13(12):1–18.

35. Palumbo, Ancona F, De Finis R, Galietti U. Experimental Study of the Crack Growth in Stainless Steels Using Thermal Methods. Procedia Engineering 2015;109:338–345.
36. Morabito AE, Chrysochoos A, Dattoma V, Galietti U. Analysis of heat sources accompanying the fatigue of 2024 T3 aluminium alloys. Int J Fatigue 2007;29(5):977−984.
37. Meneghetti G. Analysis of the fatigue strength of a stainless steel based on the energy dissipation. Int J Fatigue. 2007;29(1):81−94.
38. Boulanger T, Chrysochoos A, Mabru C, Galtier C. Calorimetric analysis of dissipative and thermoelastic effects associated with the fatigue behavior of steels. Int J Fatigue. 2006;26:221−229.
39. Stanley P. Beginnings and early development of thermoelastic stress analysis. Strain. 2008;44(4):285−287
40. La Rosa G, Risitano A. Thermographic methodology for the rapid determination of the fatigue limit of materials and mechanical components. Int J Fatigue. 2000;22(1):65−73.
41. Yang B, Liaw PK, Morrison M, et al. Temperature evolution during fatigue damage. Intermetallics. 2005;13(3−4):419−428.
42. ASTM E466 – 15. Standard Practice for Conducting Force Controlled Constant Amplitude Axial Fatigue Tests of Metallic Materials.
43. De Finis R et al 2021 IOP Conf. Ser.: Mater. Sci. Eng. 1038 012015
44. Aghayan A, Jaiswal P, Siahkoohi HR. Seismic denoising using the redundant lifting scheme. Geophysics 2016;81(3): V249-V260.
45. Chmelko V. Cyclic anelasticity of metals. Metl Mater 2014;52:353–9
46. Feltner C, Morrow J. Microplastic strain hysteresis energy as a criterion for fatigue fracture. ASME J Basic Eng Mech 1961;83:15.22.
47. Guo Q, Guo X, Fan J, Syed R, Wu C. An energy method for rapid evaluation of high-cycle fatigue parameters based on intrinsic dissipation. Int J Fatigue 2015;80:136–144